Journal of Physics: Conference Series

**PAPER** • **OPEN ACCESS**

# Multiple-degree-of-freedom actuation of rotor loads in model testing of floating wind turbines using cable-driven parallel robots

To cite this article: Valentin Chabaud *et al* 2018 *J. Phys.: Conf. Ser.* **1104** 012021

View the article online for updates and enhancements.

IOP ebooks™

Bringing you innovative digital publishing with leading voices to create your essential collection of books in STEM research.

Start exploring the collection - download the first chapter of every title for free.

This content was downloaded from IP address 129.241.191.230 on 19/02/2019 at 08:02

# Multiple-degree-of-freedom actuation of rotor loads in model testing of floating wind turbines using cable-driven parallel robots

**Valentin Chabaud[1,2], Lene Eliassen[2], Maxime Thys[2] and Thomas Sauder[2,3]**

[1]Dept. of Marine Technology, NTNU, 7491 Trondheim, Norway
[2]SINTEF Ocean, P.O. Box 4762 Torgard, 7465 Trondheim, Norway
[3]Centre for Autonomous Marine Operations and Systems (NTNU AMOS), Dept. of Marine Technology, NTNU, 7491 Trondheim, Norway

E-mail: valentin.chabaud@ntnu.no

**Abstract.** Model testing of offshore structures in ocean basins has been accepted as a necessary step for the validation and calibration of numerical models, as well as for final design checks in extreme environments. While offshore wind power makes no exception, model testing has not shown its full potential due to inherent modeling challenges. Generating highly-controlled wind fields in ocean basins and alleviating aerodynamic modeling errors due to Reynolds number mismatch in Froude-based scaling are prominent examples. To circumvent these issues, the concept of Real-Time Hybrid Model (ReaTHM) testing has been suggested by SINTEF Ocean and NTNU, Norway. Here the wind loads are no longer physically modeled but computed from online-measured motions and a numerical wind field. They are then actuated in real time on the scale model by means of actuators, while subjected to –physical- wave and current loads.

This paper aims at presenting design considerations regarding the choice of the actuator(s) and its/their interface with the scale model. The pros and cons of the chosen solution, namely cable-driven parallel robots using industrial servo drives, are presented. The focus is then directed toward the mapping between wind loads to be actuated and tension commands on each cable, called tension allocation. Two layouts corresponding to two ReaTHM testing campaigns performed in SINTEF Ocean's ocean basin are then compared on various aspects, with emphasis on tension allocation.

In addition to proving the feasibility of the chosen technical solution, results show a trade-off between flexibility (with respect among others to wind direction) and usability on other structures versus minimization of cable tensions. The latter aspect is treated in detail, using theory first adapted from literature on cable-driven parallel robots, then illustrated through relevant examples for the current application.

## 1. Introduction

Wind-wave model testing in ocean basins has become a standard in the development of floating offshore wind turbine (FWT) concepts, based on the experience from the oil & gas

Content from this work may be used under the terms of the Creative Commons Attribution 3.0 licence. Any further distribution of this work must maintain attribution to the author(s) and the title of the work, journal citation and DOI.
Published under licence by IOP Publishing Ltd

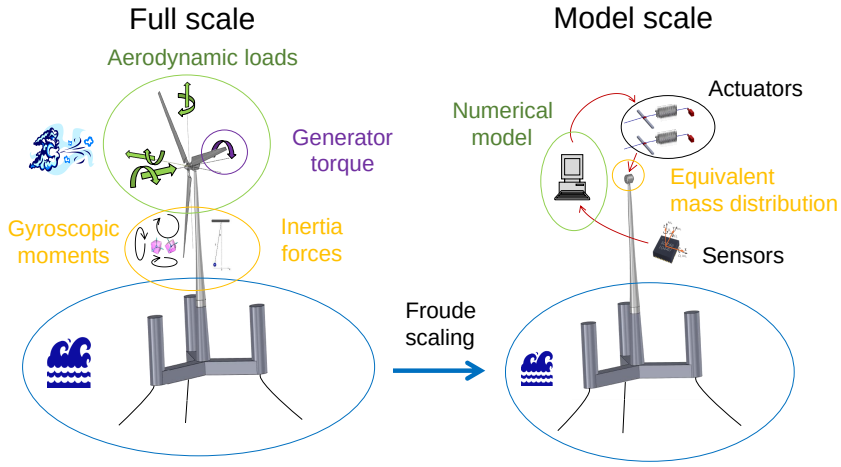


**Figure 1.** Real-time hybrid model (ReaTHM®) testing

industry. However, unlike floating oil production units, offshore wind turbines exhibit a much tighter coupling between aerodynamic and hydrodynamic loads. The necessity of an accurate simultaneous modeling of wind and wave loads poses a challenge. Generating an accurate and predictable wind field is inherently difficult in a wave basin environment [17]. Should one manage this, it would not reproduce accurate wind loads on the rotor due to a mismatch in the Reynolds number between full and model scales, as it conflicts with wave modeling imposing the Froude number to be preserved. Methods have been suggested to model the rotor thrust force in a more accurate manner [11], but the physical modeling of wind loads is still limited.

In order to address these issues, the concept of hardware-in-the-loop (HiL) testing was brought in to model testing to actuate wind loads instead of attempting to reproduce them physically. A numerical model calculates the loads in real time based on a numerical wind field and online measurements of the scale model's motions, and actuators apply them to the structure, thus closing the loop. The latter approach, illustrated in Fig. 1 for offshore wind but also relevant on other offshore structures, has been developed by SINTEF Ocean in collaboration with NTNU (see [5] and [13] for complete and concise versions, respectively) and trademarked as Real-Time Hybrid Model (ReaTHM®) testing by SINTEF Ocean AS. The first ReaTHM testing campaign for FWTs, the NOWITECH model tests, took place in fall 2015 and featured the NREL 5MW turbine mounted on the NOWITECH CSC semi-submersible [3]. A second campaign was recently completed on the OO-Star Wind Floater semi-submersible supporting the DTU 10MW turbine, tested in fall 2017 within the EU-funded LIFES50+ project [16].

This paper focuses on the design of the actuator system used in ReaTHM testing, through the comparison between the two testing campaigns presented in Sec. 3, after justifying the choice of cable-driven parallel robots in Sec. 2. The allocation problem, that is which tension to apply on which line, is then treated in Sec. 4 (theory) and Sec. 5 (application to the two designs).

## 2. Design requirements and technical solutions

Chabaud ([5], summed up in [13]) suggested a design procedure for ReaTHM testing. The earlier phases of the design set the framework before choosing actuators.

### *2.1. Force-based actuation*

The vast majority of HiL testing applications in mechanical systems uses motion actuation, which is convenient since most off-the-shelf actuators are provided with excellent motion control systems. However, for this application of ReaTHM testing, force actuation is used. The reasons

behind this choice are prone to debate and fall therefore outside the scope of this paper. This is assumed here as a specificity of the current framework, setting demanding requirements to the actuators.

### *2.2. High bandwidth and accuracy target*

One specificity of ReaTHM testing, when compared to the generic HiL testing, is the detrimental effect any dynamics in the measurement and actuation systems may have on the test outcome. As ReaTHM testing is a complement to pure hydrodynamic tests, which have benefited from decades of experience and development, the accuracy target has been set fairly high: 5% of acceptable error on quantities of interest such as platform motions or tower-base bending moments. Furthermore, this accuracy should be reached on a rather broad frequency range, called *bandwidth*. While the NOWITECH ReaTHM testing campaign set the bandwidth to wave frequency or up to 1Hz in model scale, the LIFES50+ tests increased it to blade sweeping (*3p*) frequency or up to 3-4Hz in model scale.

### *2.3. MDOF*

Among the limitations of physical modeling of wind loads in hydrodynamic laboratories introduced in Sec. 1, one particularly relevant for this paper is that non-thrust components of the aerodynamic load vector are still left to chance. Bachynski et al. [2] studied numerically the effect of not actuating a singular load component by looking at the error induced on the above-defined quantities of interest. Although the published results have been obtained using the NOWITECH concept, a similar study was performed for the OO-Star and gave similar results. It was shown that -by increasing order of importance, in addition to the thrust- the pitch moment[1], the generator torque (particularly for *constant power* above-rated control schemes), the yaw moment (particularly for the response in yaw) and the horizontal shear force should be properly modeled not to get distorted coupling with hydrodynamics. The vertical shear force could however be neglected.

### *2.4. Large workspace*

A specificity of floating offshore structures -particularly of wind turbines which exhibits large wind-induced motions- is the large required workspace, i.e. the zone where the desired range of loads can be actuated. Hall et al. [9] performed numerical simulations to obtain actuator design requirements in terms of supported motions and loads applicable to hybrid wind-wave testing of FWTs. A semi-submersible, a spar and a TLP fitted with the NREL 5MW turbine were numerically substructured to simulate a hybrid model test setup, and motion envelopes were derived. Assuming a 1:30 scaling factor (i.e that of the NOWITECH tests where the same turbine was used), displacements of up to 1m, forces of up to 40N and moments of up to 15Nm should be handled. Other information from the sensitivity studies mentioned in the previous paragraph and from observations made during the model tests themselves lead to even more conservative guidelines.

Concluding the above paragraphs, we need an actuator capable of actuating an almost full load vector of magnitude of up to 40N/15Nm at high accuracy, at a frequency of up to 3-4Hz and anywhere inside a 1m radius, 1m high cylinder.

### *2.5. Technical solutions*

A first natural idea would be to use an on-board actuator, such as fans or jets [1], to cope with the large workspace. The MDOF requirement is then a challenge, first because the mass properties

[1] Note that loads are here defined about the rotor apex, not the tower base. The thrust force does therefore not contribute to the pitch moment.

of the structure should not be altered by the weight of the actuators, but most importantly because of the accuracy and bandwidth requirements. The choice to actuate from land was then made. Looking at off-the-shelf technical solutions, MDOF robots may be split into serial robots (widely used in the industry, typically manipulators consisting of a series of arms articulated by joints) which may support -reasonably- large motions but are not able to apply large loads, and rigid-link parallel robots (such as the Stewart platform, or flexure-joint hexapod) which can apply large loads but are typically very limited in terms of handled motions. Increasing even further their inherently high cost, off-the-shelf conventional MDOF robots would therefore need to be oversized to match the required workspace specifications. Off-the-shelf MDOF robots are also likely to offer motion control only, the need for force control in the market being scarce. In-house "upgrades" of such a robot from motion to force control would imply using 1) MDOF compliant elements (see [5]) at the interface that would be very challenging to set up in practice, and 2) Taylor-made control algorithms which would typically not be compatible with the "black-box" strategy of robot manufacturers, not revealing the details of the robot's inbuilt actuators and control algorithms.

When looking at robot control techniques in the literature, the vast majority of studies deals with serial robots. Among the few studies on parallel robots, most are about Stewart platforms or similar rigid-link robots. A subcategory of parallel robots has nevertheless been rising interest in the past decade, consisting of a set of rotary actuators (typically DC motors), linked to winches pulling on cables that are linked to the end-effector at the other end. We are no longer talking about single MDOF actuators but rather about sets of 1DOF actuators. Although they may seem far away from the common image of a robot, they are referred to in the literature as *cable-driven parallel robot*s (CDPRs). They can apply large loads at high frequencies, potentially accurately, and most important they can handle very large motions, see [14, 15] for overviews.

A Taylor-made force-controlled CDPR is therefore chosen as a solution. A polyhedric frame is built at the tower top of the FWT scale model and actuator lines are attached to its corners. The actuation of rotor loads will depend highly on the design of this frame and on the actuator placement at the other end of the lines, and this is the core topic of this paper presented in the next section.

## 3. Actuation interface designs

A major particularity of CDPRs lies in the inability of cables to apply compression loads, i.e. all lines should always be kept in tension. This necessary positive offset in the tension is called here *pretension*. The most flexible and robust source of pretension is provided by actively overconstraining the frame, i.e. using more -carefully placed- actuators than load components (forces and moments) to be actuated. The number of actuators may be reduced when pretension is provided by:

- External forces on the structure, e.g. weight (when freely hanging) or stiffness (e.g. hydrostatic) combined with constant position offsets (that may be created by constant, application-specific, load offsets)
- Overconstraining with lines connected to passive elements (springs or weights) [12]
- Cable differentials, i.e. connecting several winches to the same actuators and using pulleys to direct the cables against each other [10]

The flexibility of CDPRs and the ability to modify the design between ReaTHM testing campaigns enable a trial-and-error design approach: (1) designing an actuation interface intuitively (2) verifying if it through numerical simulations (3) adjusting it if needed (4) optimizing it for the next test campaign based on observations. Two of these designs are presented in the following.

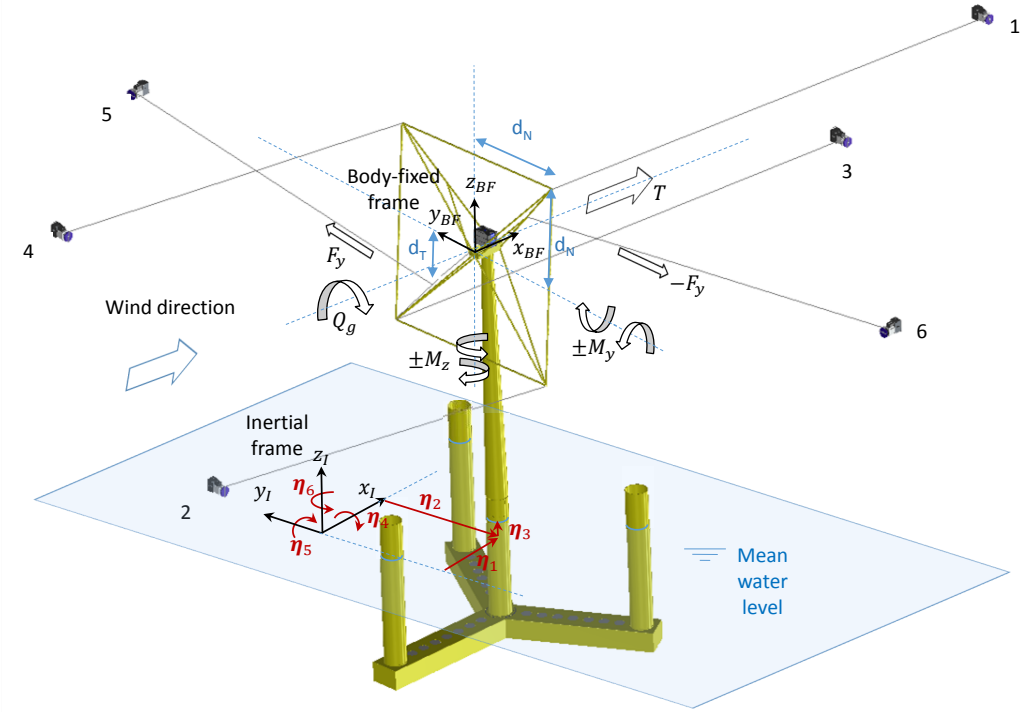


**Figure 2.** NOWITECH design, coordinate systems and notations. Motor and attachment point locations are illustrative only.

### *3.1. Actuation system for the NOWITECH tests*

The design of the NOWITECH actuation interface was based on intuitive similarity with physical wind turbine rotors. It is shown in Fig. 2, toghether with notations for coordinate systems, dimensions and the desired loads to be actuated (thrust, horizontal shear force, generator torque, pitch moment and yaw moment):

$$\boldsymbol{\tau}_{ref} = \left[\begin{array}{ccccc} T & F_y & Q_g & M_y & M_z \end{array}\right]^T$$

Its -almost planar- square pyramidal frame was

- facing wind and waves generated by the main wave maker. To model misaligned wind-wave conditions, a multi-flap wave maker on the basin side was used (30 to 150 degrees misalignment), to the cost of lower waves and more wave reflection than if the main wave maker was used.
- overconstrained only in the $(x, z)$ plane, lines 1 to 4 pulling against each other, while pretension in lines 5 and 6 was provided by a positive offset in the simulated generator torque (first alternative solution in the list above). Strictly speaking the thrust also provides such an offset, and three lines pulling in the wind direction could be sufficient to apply thrust force, pitch and yaw moments, removing the need for one line. However, based on numerical simulations, an arm of no less than nine meters would then be necessary to actuate pitch and yaw moments. The offset in torque being present only in turbine operating conditions, tests with no wind (called *following mode*, with non-zero line tensions but actuating no neat load), parked conditions or faults such as grid loss were performed by adding an artificial offset with no physical meaning, inducing a small error.
- centered at the hub location and featuring a 5 degrees tilt as the original rotor. SINTEF Ocean's basin being 80m long, jacket structures were installed in order to bring motors closer to the model (see Fig. 3), and thus keep them at acceptable heights.

- made of aluminum tubes, originally 2m wide and high ($2d_N$ in Fig. 2), but reduced to 1m for stiffening. Although feedback control and its stability are not the topic of this paper (see [5] for details), the eigenmodes and frequencies of the frame showed to be a major design driver.

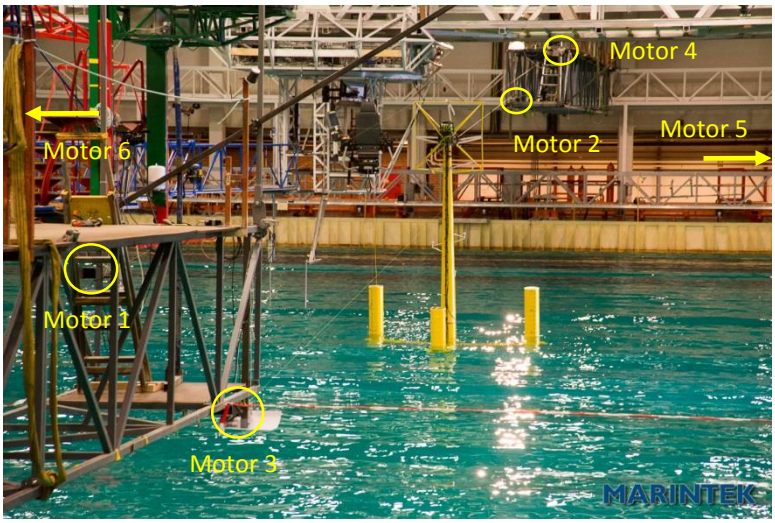


**Figure 3.** NOWITECH design in SINTEF's ocean basin

The main advantage of this first design may be the physical meaning of each line's contribution to the rotor loads. While this will be thoroughly treated in Sec. 4 and 5, it may be approximated[2] and summed up elegantly as in Tab. 1, where $\bar{F}$ is a reference tension driving pretension in lines 1-4, and $\eta_6$ is the -assumed small- yaw angle (other motions having less impact). Based on these relationships between line tensions and loads, it is easy to derive design requirements on the dimensions $d_N$ and $d_T$ and reference tension $\bar{F}$ given a desired range of load amplitudes.

| Line nr | Function | Simplified expression |
|---|---|---|
| 1 | Thrust force + Pitch moment + Pretension | $\frac{T}{2} + \frac{M_y}{2d_N} + \bar{F} + \eta_6\left(-\frac{F_y}{2} + \frac{Q_g}{2d_T}\right)$ |
| 2 | Pitch moment - Yaw moment + Pretension | $\frac{M_y}{2d_N} - \frac{M_z}{2d_N} + \bar{F}$ |
| 3 | Thrust force - Yaw moment + Pretension | $\frac{T}{2} - \frac{M_z}{2d_N} + \bar{F} + \eta_6\left(-\frac{F_y}{2} - \frac{Q_g}{2d_T}\right)$ |
| 4 | Pretension | $\bar{F}$ |
| 5 | Generator torque + Shear force | $\frac{F_y}{2} + \frac{Q_g}{2d_T} + \eta_6\left(-\frac{T}{2} + \frac{M_y}{2d_N}\right)$ |
| 6 | Generator torque - Shear force | $-\frac{F_y}{2} + \frac{Q_g}{2d_T} + \eta_6\left(\frac{T}{2} + \frac{M_y}{2d_N}\right)$ |

**Table 1.** Contribution of each line to rotor loads, NOWITECH design

### *3.2. Actuation system for the LIFES50+ tests*

To address the shortcomings listed in Sec. 3.1, the square pyramidal shape was replaced by the twisted triangular prism shown in Fig. 4, which was:

[2] Linearized around 0 position

- centered at the tower top rather than at the hub. The rotational symmetry enables changing the wind direction at will independently on the waves. As a drawback, rotational symmetry implies that the center of mass of the rotor-nacelle assembly has to be assumed to be located on the yaw axis. Else additional inertia loads have to actuated, which is a challenge in practice.
- fully overconstrained thanks to rotational symmetry, the pretension in yaw being provided by the twisted feature.
- upright (rather than tilted), enabling actuation from the basin sides. This has two advantages: 1) greatly lowering installation time and improving access to the motors and 2) increasing the performance of the limited actuation strategy: As the body-fixed vertical shear force is not actuated, it is replaced by a parasitic -mostly restoring- force induced by the tensioned lines. Depending on the attitude of the floater, the effect of this parasitic force will be split between the surge and heave degrees of freedom. Removing tilt increases the fraction of this parasitic force that has negligible effect in the overall response (aligned with the -by several orders of magnitude- larger axial tower stiffness and buoyancy), and decreases the fraction of the parasitic force which deteriorates the tower-base bending moment, surge and pitch motions. The drawback is longer lines as seen in Tab. 2, which sets additional challenges for tension control [5].
- stiffer than the square pyramid thanks to its geometry (lower aspect ratio, lines pulling on beams axially rather than transversely and on nodes of the most significant frame eigenmodes rather than between them) and material (carbon fiber).

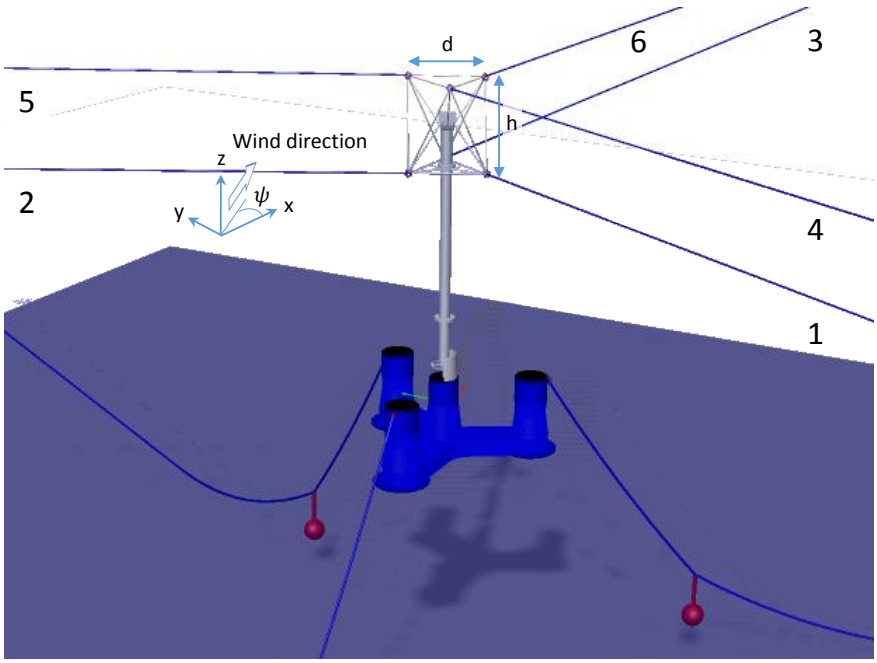


**Figure 4.** LIFES50+ design

| Line nr | 1 | 2 | 3 | 4 | 5 | 6 |
|---|---|---|---|---|---|---|
| NOWITECH | 18.5 | 16.3 | 18.4 | 16.2 | 23.1 | 26.4 |
| LIFES50+ | 27.4 | 27.1 | 31.6 | 27.1 | 27.4 | 31.6 |

**Table 2.** Line lengths when the model is at origin, in meters

The design requirements for pretension and dimensions may then be derived from the simplified expression for the commanded tension on line $i$

$$\begin{aligned}\mathbf{F}_{ref_i} \approx & \frac{\cos\left(\psi + \frac{2i\pi}{3}\right)}{3} T - \frac{\sin\left(\psi + \frac{2i\pi}{3}\right)}{3} F_y + \\ & (-1)^{\lfloor \frac{i+2}{3} \rfloor} \left[ \frac{2\sin\left(\psi + \frac{2i\pi}{3}\right)}{3h} Q_g + \frac{2\cos\left(\psi + \frac{2i\pi}{3}\right)}{3h} M_y + \frac{1}{\sqrt{3}d} M_z \right] + \bar{F}\end{aligned} \tag{1}$$

where $\psi$ is the wind direction.

Although the design of each concept is intuitive, detailed work is needed to proove their feasibility, which may be adapted from literature on CDPRs and is presented in the following sections.

## 4. Tension allocation: theoretical background

The control of the tension setpoints on each line as a function of the resulting *wrench* (here rotor load vector, according to the terminology used in robotics) at the *end-effector* (here frame) is in this paper referred to as *tension allocation*. Among the studies on cable-driven parallel robots found in the literature, few deal with force (tension) control [3] (which includes both allocation and tracking). However, efficient motion-control algorithms make use of the tension setpoints (though they do not deal with their effective tracking) for compensation of the static and dynamic responses of the system. Consequently the topic of tension allocation is relatively well covered and adapted to the current application in this section.

### *4.1. Wrench matrix*

Let $\mathbf{p}_i^{BF}$ be the coordinates of the $i^{th}$ out of $n$ attachment point in body-fixed coordinates, the origin being defined by the reference point of the load vector (see Fig. 2). Moving to the inertial frame, it reads

$$\mathbf{p}_i^I = \mathbf{R}_I^{BF}\left(\boldsymbol{\eta}_{4..6}\right)\ \mathbf{p}_i^{BF} + \boldsymbol{\eta}_{1..3} \tag{2}$$

with $\boldsymbol{\eta}_{1..3}$ the position of the above-defined origin in global coordinates, $\boldsymbol{\eta}_{4..6}$ the attitudes defined by roll, pitch and yaw Euler angles (as in Fig. 2) and $\mathbf{R}_I^{BF}$ the rotation matrix from body-fixed to inertial frames built from attitudes, in this application in the yaw-pitch-roll order. Given the motor coordinates in the inertial frame $\mathbf{p}_M^I$, the cable length $l_i$ of actuator $i$ reads

$$l_i = ||\mathbf{p}_{M_i}^I - \mathbf{p}_i^I|| \tag{3}$$

and the line's unitary direction vector in body-fixed coordinates $\mathbf{e}_{N_i}^{BF}$

$$\mathbf{e}_{N_i}^{BF} = \mathbf{R}_I^{BF^T} \frac{\mathbf{p}_{M_i}^I - \mathbf{p}_i^I}{l_i} \tag{4}$$

[3] Those who do are typically interested in hybrid motion-force control, where force control is done in a qualitative fashion such as manipulating objects with enough force to ensure grip and not too much to avoid damaging

Let now $\boldsymbol{\tau}$ be the wrench (actuated load vector) and $\mathbf{F}$ the vector of line tensions. They are linked through the $6 \times n$ wrench matrix $\mathbf{J}$ by

$$\boldsymbol{\tau} = \mathbf{J}\left(\boldsymbol{\eta}\right) \mathbf{F} \tag{5}$$

the columns of $\mathbf{J}$ being then defined by

$$\mathbf{J}_i\left(\boldsymbol{\eta}\right) = \begin{bmatrix} \mathbf{e}_{N_i}^{BF} \\ \mathbf{S}\left(\mathbf{p}_i^{BF}\right) \mathbf{e}_{N_i}^{BF} \end{bmatrix} \tag{6}$$

with $\mathbf{S}\left(\,\right)$ the cross product-equivalent matrix reading $\mathbf{S}\left(\mathbf{x}\right) \mathbf{y} = \mathbf{x} \times \mathbf{y}$, $\forall \left(\mathbf{x}, \mathbf{y}\right) \in \mathbb{R}^{3\times 2}$.

*4.2. Allocation problem*

The allocation problem consists in determining which line tensions $\mathbf{F}_{ref}$ should be applied to obtain the desired subwrench $\boldsymbol{\tau}_{ref}$ of length $m \leq 6$ (possibly removing some undesired components). In other words,

$$find \;\; \mathbf{F}_{ref}\left(\boldsymbol{\tau}_{ref}, \boldsymbol{\eta}\right) \;\; which\ yields \;\; \mathbf{P}\,\boldsymbol{\tau}_{ref} = \mathbf{P}\,\mathbf{J}\left(\boldsymbol{\eta}\right) \mathbf{F}_{ref} \tag{7}$$

with $\mathbf{P}$ a $m \times 6$ selector matrix (the $6 \times 6$ identity matrix whose rows corresponding to the undesired components are removed). For most classical (fully constrained) robots, a regular inversion of $\mathbf{P}\,\mathbf{J}\left(\boldsymbol{\eta}\right)$ would be used. As CDPRs are typically overconstrained (due to the no-slack condition on the cables), the system of equations is underdetermined and its solution set (if any, see 4.4) is given by

$$\mathbf{F}_{ref} = \left(\mathbf{P}\,\mathbf{J}\left(\boldsymbol{\eta}\right)\right)^{+} \mathbf{P}\,\boldsymbol{\tau}_{ref} + \left[\mathbf{I} - \left(\mathbf{P}\,\mathbf{J}\left(\boldsymbol{\eta}\right)\right)^{+} \mathbf{P}\,\mathbf{J}\left(\boldsymbol{\eta}\right)\right] \mathbf{W} \tag{8}$$

with $^{+}$ designating the Moore-Penrose pseudo-inverse operator (see for instance [14] for properties, [6] for a deeper insight) and $\mathbf{I}$ the $n \times n$ identity matrix. $\mathbf{W}$ is an arbitrary vector in $\mathbb{R}^n$ that once multiplied by the matrix characterizing the nullspace of $\mathbf{P}\,\mathbf{J}\left(\boldsymbol{\eta}\right)$, i.e. $\left[\mathbf{I} - \left(\mathbf{P}\,\mathbf{J}\left(\boldsymbol{\eta}\right)\right)^{+} \mathbf{P}\,\mathbf{J}\left(\boldsymbol{\eta}\right)\right]$ -that has $m$ dependent rows- will give a vector with $n - m$ independent elements. Assuming that we do not need more than one more line than there are desired wrench components, we assume

$$n = m + 1 \tag{9}$$

for the rest of this study, to minimize complexity and cost. (8) becomes then an underdetermined system of rank 1, and may be rewritten as

$$\mathbf{F}_{ref} = \left(\mathbf{P}\,\mathbf{J}\left(\boldsymbol{\eta}\right)\right)^{+} \mathbf{P}\,\boldsymbol{\tau}_{ref} + \left[\mathbf{I} - \left(\mathbf{P}\,\mathbf{J}\left(\boldsymbol{\eta}\right)\right)^{+} \mathbf{P}\,\mathbf{J}\left(\boldsymbol{\eta}\right)\right] \mathbf{1}_{6\times 1} w = \mathbf{b}\left(\boldsymbol{\tau}_{ref}, \boldsymbol{\eta}\right) + \mathbf{a}\left(\boldsymbol{\eta}\right) w \tag{10}$$

where the $n$ dependent elements in the second term of the right-hand side have been merged into one single scalar $w \in \mathbb{R}$ multiplied with the column array of ones $\mathbf{1}$, and $\left(\mathbf{a}, \mathbf{b}\right) \in \mathbb{R}^{n\times 2}$ have been introduced for conciseness. This gives a physical meaning to the general solution, as $w$ is tightly related to the concept of pretension, as we will see in the following.

*4.3. Allocation strategies*

The allocation problem is now reduced to how to choose $w$. This choice may be based upon:

(i) Keeping line tensions as close as possible to a reference tension $\bar{F}$, for instance to minimize internal load variations in the structure or to limit averaged variations in line properties

(e.g. natural frequencies). This is equivalent to solving an optimization problem minimizing the Euclidean ($L_2$) norm :

$$find \underset{\mathbf{F}_{ref}(w)}{min} \left( \sqrt{\left(\mathbf{F}_{ref} - \bar{F}\,\mathbf{1}_{n\times1}\right)^T \left(\mathbf{F}_{ref} - \bar{F}\,\mathbf{1}_{n\times1}\right)} \right) \; subject\ to \;\; \mathbf{P}\,\boldsymbol{\tau}_{ref} = \mathbf{P}\,\mathbf{J}\,(\boldsymbol{\eta})\,\mathbf{F}_{ref} \tag{11}$$

which, when removing the square root, is a quadratic problem (hence convex) whose unique solution in terms of $w$ is found by using (10), which satisfies the constraint in (11) which then breaks down to

$$\frac{\partial \left(\mathbf{b} + \mathbf{a}w - \bar{F}\,\mathbf{1}_{n\times1}\right)^T \left(\mathbf{b} + \mathbf{a}w - \bar{F}\,\mathbf{1}_{n\times1}\right)}{\partial w} = 0 \tag{12}$$

Using the properties of the pseudo-inverse [14] which is known to minimize the Euclidean norm, it is easy to show that $\mathbf{a}^T\mathbf{a} = \mathbf{a}^T\,\mathbf{1}_{n\times1}$ and $\mathbf{a}^T\mathbf{b} = \mathbf{b}^T\mathbf{a} = 0$, hence

$$w = \bar{F} \tag{13}$$

This may be the most straight-forward approach, used by default, due to its direct relation to the pseudo-inverse matrix which greatly facilitates its implementation, and to the direct physical meaning of $w$.

(ii) Keeping line tensions as far as possible from user-defined lower and upper bounds. The aim is then to limit the span of variations in line properties or to keep some margin from slack or excessive tension in case of overshoots in tension control or high-frequency vibrations. As pointed out by Gosselin et al. [7] who suggested this approach, this may be more relevant than keeping tensions close to a reference for most CDPRs applications, and ReaTHM testing on FWTs makes no exception. This amounts to solving a similar optimization problem to (11), but this time using the infinity ($L_\infty$) norm

$$\left|\left|\mathbf{F}_{ref} - \bar{F}\,\mathbf{1}_{n\times1}\right|\right|_\infty = \underset{i}{max}\left|\mathbf{F}_{ref_i} - \bar{F}\right| \tag{14}$$

However the problem becomes linear and the solution may therefore be discontinuous. To ensure continuity, [7] used as a close approximation higher-order ($L_p$) norms

$$\left|\left|\mathbf{F}_{ref} - \bar{F}\,\mathbf{1}_{n\times1}\right|\right|_p = \left(\sum_{i=1}^{n}\left(\mathbf{F}_{ref_i} - \bar{F}\right)^p\right)^{\frac{1}{p}} \tag{15}$$

which converge toward (14) when $p \to \infty$. Unlike for the Euclidean norm with the Moore-Penrose pseudo-inverse, there does not exist any generalized inverse independent on $\boldsymbol{\tau}_{ref}$ that minimizes $L_p$ norms with $p$ larger than 2 [6], so no such simple solution as (13) can be derived. [7] started from (7) and used the tension on one particular line to characterize the nullspace, and made heavy use of symbolic solvers. Instead, we use here the framework defined by (10) and solve numerically for $w$ by finding the roots of a polynomial:

$$\frac{\partial \left(\sum_{i=1}^{n}\left(\mathbf{b}_i + \mathbf{a}_i w - \bar{F}\right)^p\right)}{\partial w} = p\sum_{i=1}^{n}\mathbf{a}_i\left(\mathbf{b}_i + \mathbf{a}_i w - \bar{F}\right)^{p-1} = 0 \tag{16}$$

which admits a unique real solution when $p$ is even, due to the convexity of the problem. It can be verified that $p = 2$ leads to $w = \bar{F}$ as expected.

(iii) Specifying the tension $\mathbf{F}_{ref_k}$ on one particular line $k$ satisfying $\mathbf{a}_k \neq 0$, typically to be able to make this line passive (replacing the actuator by a spring or cable differential, measuring the tension and specifying it as input to the allocation problem) or to give insight (physical meaning) to the tension allocation process. In this case the pretension is simply given by

$$w = \frac{\mathbf{F}_{ref_k} - \mathbf{b}_k}{\mathbf{a}_k} \tag{17}$$

### *4.4. Workspace constraints*

The workspace is defined in the CDPR literature as the set of reachable end-effector poses in motion-controlled CDPRs. In the current force control framework, we may extend this definition to the set of feasible desired wrenches $\mathbf{P}\boldsymbol{\tau}_{ref}$ given a pose $\boldsymbol{\eta}$. Various solutions to (7) have been given in (13), (16) and (17), but their existence is actually not guaranteed and depends on $\mathbf{P}\,\mathbf{J}\,(\boldsymbol{\eta})$ and thus on the workspace. Workspace limitations have given birth to advanced mathematical representations in the literature [8, 4]. Here, consistently with the trial-and-error approach introduced in Sec. 3, a simple workspace representation is used and its limitations are presented in the following together with design guidelines.

*Unconstrained problem* A solution to (7) exists (in which case it is given by (8)) if and only if the vector $\mathbf{P}\boldsymbol{\tau}_{ref}$ is included in the space described by $\mathbf{P}\,\mathbf{J}\,(\boldsymbol{\eta})$, i.e. if and only if

$$rank\left(\mathbf{P}\left[\begin{array}{cc} J\,(\boldsymbol{\eta}) & \boldsymbol{\tau}_{ref} \end{array}\right]\right) = rank\left(\mathbf{P}\,\mathbf{J}\,(\boldsymbol{\eta})\right) \tag{18}$$

-known as the Rouché-Capelli theorem- which may be verified by using a symbolic solver.

In practice, rank deficiency is avoided if there does not exist any point (an end-effector pose) in the workspace where all lines are normal to the axis of a desired, non-0 force component or parallel to the axis of a desired, non-0 moment component.

*Constrained problem* The rank condition above does not take tension constraints (no-slack and excessive tension) into account. In practice, the existence of a solution (10) verifying

$$F_{min}\,\mathbf{1}_{n\times 1} \leq \mathbf{F}_{ref} \leq F_{max}\,\mathbf{1}_{n\times 1} \tag{19}$$

is required, with $F_{min}$ and $F_{max}$ user-defined positive lower and upper bounds respectively. In general, $w$ has a positive effect on tension (i.e. $\mathbf{a}_i > 0$), however in case of large motions compared with line lengths this effect might be negative on some lines, and constraints on $w$ corresponding to (19) should be split upon the sign of $\mathbf{a}_i$. These constraints may be then written as:

$$w_{min} = max\left(\underset{\{\mathbf{a}>0\}}{max}\left(\frac{F_{min}\,\mathbf{1}_{n\times 1}-\mathbf{b}}{\mathbf{a}}\right),\ \underset{\{\mathbf{a}<0\}}{min}\left(\frac{F_{max}\,\mathbf{1}_{n\times 1}-\mathbf{b}}{\mathbf{a}}\right)\right) \tag{20}$$

$$w_{max} = min\left(\underset{\{\mathbf{a}>0\}}{min}\left(\frac{F_{max}\,\mathbf{1}_{n\times 1}-\mathbf{b}}{\mathbf{a}}\right),\ \underset{\{\mathbf{a}<0\}}{max}\left(\frac{F_{min}\,\mathbf{1}_{n\times 1}-\mathbf{b}}{\mathbf{a}}\right)\right) \tag{21}$$

giving the set of solutions $(w, \mathbf{b})$ at a given pose $\boldsymbol{\eta}$

$$\begin{cases} w_{min}\left(F_{min}, F_{max}, \underset{\{\mathbf{a}_i\neq 0\}}{\mathbf{b}}\right) \leq \quad w \quad \leq w_{max}\left(F_{min}, F_{max}, \underset{\{\mathbf{a}_i\neq 0\}}{\mathbf{b}}\right) \\ \qquad\qquad F_{min} \leq \underset{\{\mathbf{a}_i=0\}}{\mathbf{b}} \leq F_{max} \end{cases} \tag{22}$$

If $w_{min} > w_{max}$ or if the bottom inequality in (22) does not hold, no solution exists. In practice, the former is avoided when the scale model stays well inside (far from the relevant faces of) the polyhedron defined by actuator locations (so that there exists a reasonably high $w$ such that $\mathbf{F}_{ref} \geq F_{min}$) , and the actuators are correctly dimensioned (so that $F_{max}$ is large enough to verify $\mathbf{F}_{ref} \leq F_{max}$). The latter is avoided when any line that is not overconstrained is provided with pretension through constant wrench offsets or external forces, as presented in the introduction of Sec. 3.

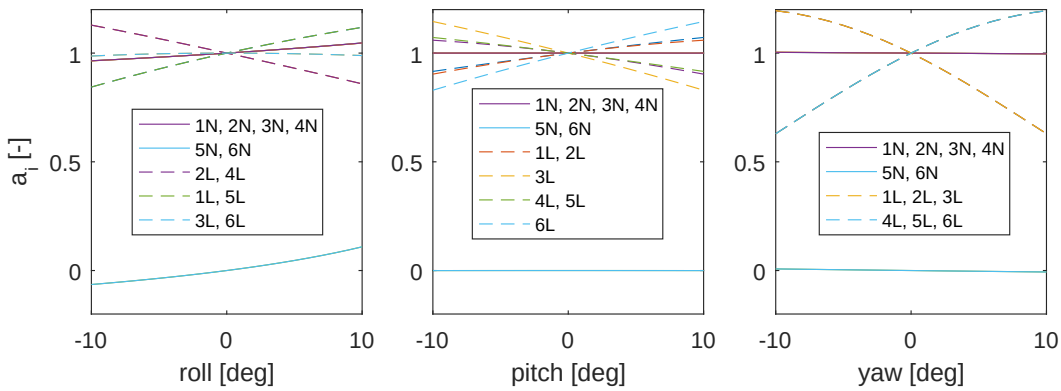


**Figure 5.** Variations of the components of $\mathbf{a}$ with elementary rotations. Legend: line nr followed by N: NOWITECH or L:LIFES50+

## 5. Tension allocation: applications

This section aims at illustrating the allocation theory of Sec. 4 applied to the two concepts described in Sec. 3. Sec. 5.1 aims at illustrating qualitatively the effect of pretension, end-effector pose and desired wrench on commanded line tensions, while Sec. 5.2 uses the norm of the commanded tension vector for a more quantitative comparison between designs and allocation strategies.

### *5.1. Pretension and workspace*

*5.1.1. Nullspace analysis* To illustrate the effect of $w$ on the pretension on the two designs, one may look at $\mathbf{a}$ (the vector characterizing the nullpace) as a function of the pose $\boldsymbol{\eta}$. Looking at Fig. 5 we observe that

- $\mathbf{a}_i > 0$ and $\mathbf{a}_i \approx 1$ ($\mathbf{a}_i(\boldsymbol{\eta} = 0) = 1$) for overconstrained lines (i.e. whose number is higher than that of the wrench components they are meant to apply) i.e. for all lines of the LIFES50+ design (which still necessitate adjustments of $w$ to compensate for changes in the frame orientation), and for lines 1-4 of the NOWITECH design. In other words, $w$ is close to the pretension itself, and it has the same effect on all lines. This prevents any excessively large value for $w_{min}$ and therefore guarantees the existence of a solution to (19), assuming the desired loads are of reasonable amplitude.
- $\mathbf{a}_i(\boldsymbol{\eta} = 0) = 0$ for fully constrained lines (i.e. which lack the redundancy of overconstrained lines), i.e. lines 5-6 of the NOWITECH design. In this case $w$ slightly affects but is not the main source of pretension (it does not affect it at all when $\boldsymbol{\eta} = 0$). The bottom condition in (22) drives then the existence of a solution to (19).

These observations are valid as long as the model stays far from the edges of the polygon defined by actuator locations in the $(x, y)$ plane (comparing the line lengths of Tab. 2 and the workspace requirements of Sec. 2), and the angle variations in roll and pitch are small[4] so that the effect of the $z$ dimension remains negligible.

*5.1.2. Workspace analysis* To understand how the allocation scheme works, it is interesting to investigate the variations in line tensions 1) for varying pose $\boldsymbol{\eta}$ and/or 2) for varying desired loads $\boldsymbol{\tau}_{ref}$. The latter may be treated using the simplified relationships between wrench and tensions linearized about $\boldsymbol{\eta} = 0$ given in Tab. 1 and (1). The former is illustrated in the following

[4] The dependency of allocation on rotations remains significant, while the dependency on translations have much less impact due to the above-stated polygon size and shape

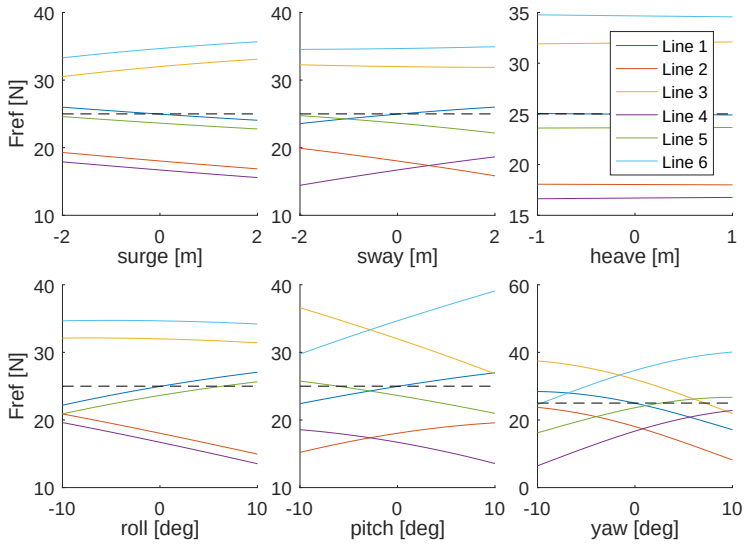


**Figure 6.** Variation of line tensions about the pretension (dashed line) induced by elementary platform motions when applying average rotor loads at rated wind speed (LIFES50+ setup)

for the LIFES50+ case using the Euclidean norm-minimization strategy (choice (i) in Sec. 4.3). The desired wrench is set to $\mathbf{P}\boldsymbol{\tau}_{ref} = \begin{bmatrix} 25\,N & 0\,N & 6\,Nm & 2\,Nm & 0\,N \end{bmatrix}^T$, corresponding to the largest average aerodynamic loads, occuring at rated wind conditions. Pretension is set to $\bar{F} = 25N$. Variations in $F_{ref}$ with motions are shown in Fig. 6 and Fig. 7. It is seen that:

- Within the bounds defined in Sec. 2, the variations with horizontal translations are rather small for the same reasons as given in Sec. 5.1.1. Larger variation in horizontal offsets are included in Fig. 7 as a representation of the effect of shorter lines, for instance due to space constraints in smaller basins.
- Line tensions are fairly independent on vertical translation.
- The effect of rotations -especially in yaw- is sharper. The lower bound $F_{min}$ may be reached in specific rotation combinations.

### *5.2. Norms and allocation strategies*

The two designs and the various allocation strategies described by (i), (ii) and (iii) in Sec. 4.3 have been compared by looking at the Euclidean and infinite norms of the line tension vector $\mathbf{F}_{ref}$ , seen as interesting performance indicators. The following settings were used in the analysis:

- The reference tension $\overline{F}$ was set to 25N, and the lower bound $F_{min}$ at 5N
- The $L_6$ norm ($p = 6$) was chosen to approximate $L_\infty$ in strategy (ii).
- The allocation strategy (iii) has been considered only in the NOWITECH case. It was indeed the chosen strategy for the NOWITECH ReaTHM tests, following the intuitive allocation of Tab. 1 by setting $F_{ref_4} = \overline{F}$. Strategy (i) was used for LIFES50+ tests, and emphasis has been put here on the comparison with strategy (ii).
- To make comparison meaningful, loads and motions computed/measured during the LIFES50+ ReaTHM tests are used on both designs, i.e. we consider the hypothetical situation where the NOWITECH actuation interface (line ends locations) was used in LIFES50+ tests.

Two relevant load cases [16] have been selected for illustration:

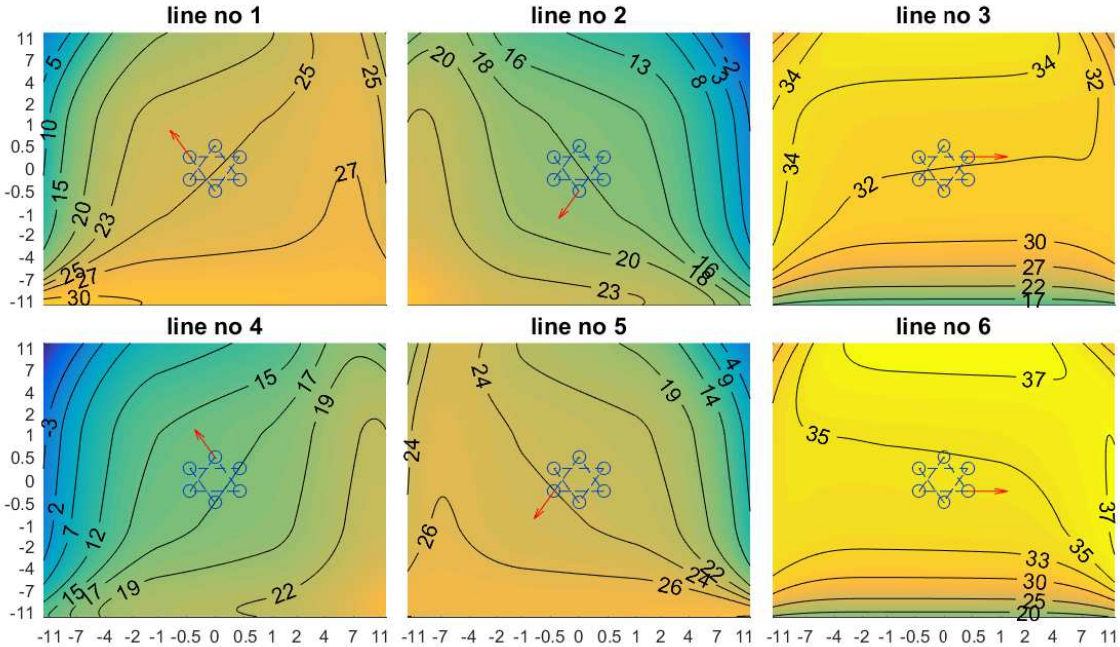


**Figure 7.** Tension contours [N] as a function of the position of the model in the horizontal plane [m], with other position components set to 0 (LIFES50+ setup)

*Extreme coherent directional change in rated (wind speed 11.4 m/s) operating conditions,* which within a short time lapse shows both the largest mean values and large transients in rotor loads and motions. Results are shown in Fig. 8.

- Regarding the NOWITECH design, it is not surprising to see that allocation scheme (iii) (based on keeping tension constant on one particular line) leads to higher norms than if a minimization scheme were used. However, the choice of the norm does not seem to influence the result much. This could have been expected from Tab. 1, attributing a clear function to each line and therefore limiting the potential of spreading tensions over lines. Moreover, Fig. 5 tells that only negligible adjustments in pretension are needed when the model orientation changes, showing a limited effect of $w$ in (10) and therefore of any optimization.
- Regarding the LIFES50+ design, it is first seen that norms are higher than for NOWITECH when using the same allocation strategy. While this could be expected from the frame geometry, the large extent (up to 50% increase) is an interesting result that is attributed to the difference in sensitivity of the pretension on the pitch angle, as seen in Fig. 5. Another interesting result lies in the observation that minimizing the $L_6$ norm does not affect much the $L_2$ norm, while it significantly lowers the $L_\infty$ one.

| | $min\,(L_2)$ N | $min\,(L_6)$ N | $F_{ref_4} = \overline{F}$ N | $min\,(L_2)$ L | $min\,(L_6)$ L |
|---|---|---|---|---|---|
| $\frac{\sum_{i=1}^{6} std(\mathbf{F}_{ref_i})}{6}$ | 1.56 N | 1.66 N | 1.82 N | 2.32 N | 2.49 N |
| $max\,(\mathbf{F}_{ref})$ | 36.7 N | 36.0 N | 47.2 N | 41.8 N | 40.8 N |
| $min\,(\mathbf{F}_{ref})$ | 11.6 N | 13.8 N | 16.8 N | 5.00 N | 7.56 N |

**Table 3.** Statistical properties of line tensions in near-cutout operating conditions with various allocation strategies. N: NOWITECH L: LIFES50+.

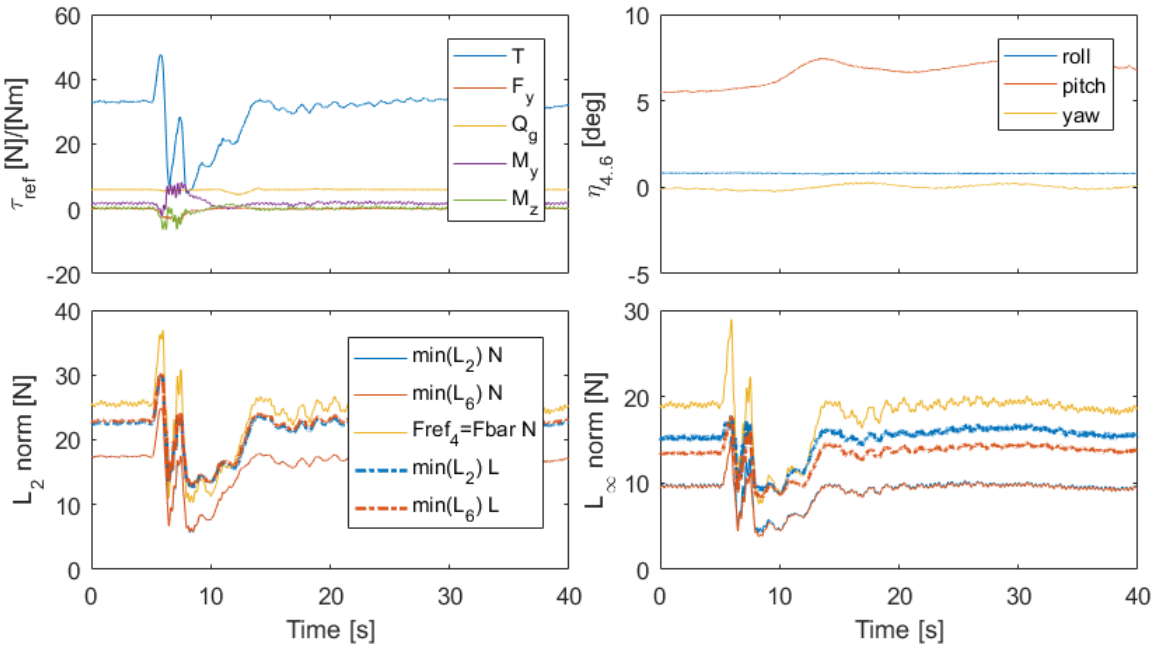


**Figure 8.** Rotor loads and induced FWT motions (upper row) and $L_2$ and $L_\infty$ norms of the commanded tension vector for various setups and allocation schemes (bottom row) in extreme coherent directional change in rated conditions. N: NOWITECH L:LIFES50+.

*Near-cutout (wind speed 25 m/s) operating conditions,* featuring the largest standard deviations of rotor loads and motions. Results are shown in Fig. 9 and Tab. 3.

- The observations made above are confirmed. Pitch and yaw motions, large at their natural frequencies (also at the surge frequency for pitch due to the strong coupling) and generally at low frequencies where the wind spectrum (averaged over the rotor area) has most energy, induce much larger line tensions with the LIFES50+ setup than with the NOWITECH one.
- A lower reference tension could be used with the NOWITECH design, and using minimization strategies would significantly lower peak tensions (see second row in Tab. 3).
- Using $L_6$ instead of $L_2$ as the objective function to be minimized would keep lines further away from any slack event for the LIFES50+ design (we can see in Tab. 3 that at least one line at at least one point in time had to be coerced to the lower bound when using minimization of the $L_2$ norm). As it leads to a negligible increase in standard deviations of line tensions (first row in the table), the second allocation strategy should be preferred to the first one (unless computational time shows to be limiting).

## 6. Conclusion

After having introduced the need for hardware–in-the-loop testing of floating wind turbines in ocean basins and justifying the use of cable-driven parallel robots for actuating rotor loads, two design of actuator setup were described. While the NOWITECH design focused on similarities with a physical rotor, the LIFES50+ design showed enhanced flexibility, among other improvements. Tension allocation -or how to split the rotor loads across the actuator lines- was then derived from methods applied earlier for cable-driven parallel robots. In particular, emphasis was put on how to choose line pretension. The underlying theory was illustrated through workspace analyses and case studies. The increased flexibility of the LIFES50+ design, despite the longer lines, comes to the cost of higher line tensions compared to the NOWITECH

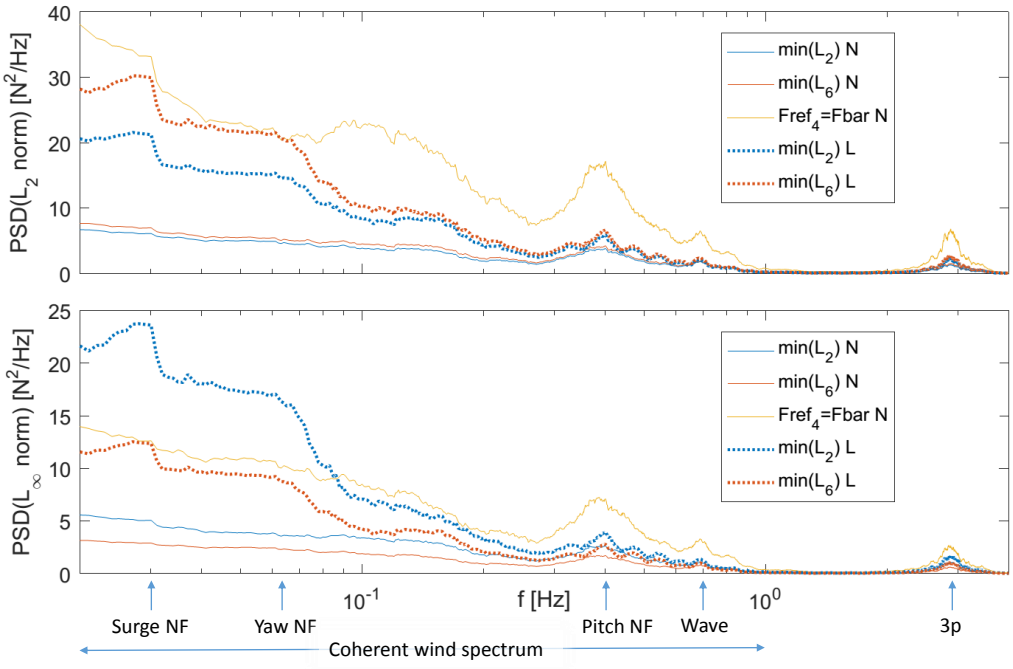


**Figure 9.** Power spectral densities of the $L_2$ and $L_\infty$ norms of $\mathbf{F}_{ref}$ in near-cutout operating conditions with various allocation strategies. N: NOWITECH L: LIFES50+. NF: natural frequency.

design. Seeking to minimize the norm of the line tension vector is therefore crucial in the LIFES50+ case. To minimize the probability of near-slack or excessive tensions, higher-order norms than the Euclidean one should be used, despite the convenience of the latter one when it comes to implementation.

## Acknowledgments
The present work was supported by

- the Research Council of Norway through the project No. 254845/O80 "Real-Time Hybrid Model Testing for Extreme Marine Environments", and through the Norwegian Research Center for Offshore Wind Technology (NOWITECH), contract No. 193823.
- the European Union's Horizon 2020 research and innovation programme through the LIFES50+ project under grant agreement No. 640741.

, support which is hereby gratefully acknowledged. Also, we are grateful to Dr. techn. Olav Olsen AS for the permission and contribution to set up the public 10MW semi-submersible design based on their concept of the OO-Star Wind Floater (`www.olavolsen.no`).

## References
[1] José Azcona, Faisal Bouchotrouch, Marta González, Joseba Garciandía, Xabier Munduate, Felix Kelberlau, and Tor A Nygaard. Aerodynamic Thrust Modelling in Wave Tank Tests of Offshore Floating Wind Turbines Using a Ducted Fan. *Journal of Physics: Conference Series*, 524:012089, June 2014.

[2] Erin E. Bachynski, Valentin Chabaud, and Thomas Sauder. Real-time Hybrid Model Testing of Floating Wind Turbines: Sensitivity to Limited Actuation. *Energy Procedia*, 80:2–12, 2015.

[3] Erin E. Bachynski, Maxime Thys, Valentin Chabaud, Thomas Sauder, and Lars O. Sæther. Real-time Hybrid Model Testing of a Braceless Semi-submersible Wind turbine. Part II: Experimental Results. In *Proc. of 35th OMAE conf.*, 2016.

[4] Samuel Bouchard, Clément Gosselin, and Brian Moore. On the ability of a cable-driven robot to generate a prescribed set of wrenches. *Journal of Mechanisms and Robotics*, 2(1):011010, 2010.

[5] Valentin Chabaud. *Real-Time Hybrid Model Testing of Floating Wind Turbines*. Phd thesis, NTNU, 2016.

[6] Ivan Dokmanić and Rémi Gribonval. Beyond moore-penrose part i: Generalized inverses that minimize matrix norms. *arXiv preprint arXiv:1706.08349*, 2017.

[7] Clément Gosselin and Martin Grenier. On the determination of the force distribution in overconstrained cable-driven parallel mechanisms. *Meccanica*, 46(1):3–15, 2011.

[8] Marc Gouttefarde. Characterizations of fully constrained poses of parallel cable-driven robots: a review. In *Proceedings of the ASME Mechanisms and Robotics Conference*, 2008.

[9] Matthew Hall, Andrew Goupee, and Jason Jonkman. Development of performance specifications for hybrid modeling of floating wind turbines in wave basin tests. *Journal of Ocean Engineering and Marine Energy*, pages 1–23, 2017.

[10] Hamed Khakpour, Lionel Birglen, and Souheil-Antoine Tahan. Synthesis of differentially driven planar cable parallel manipulators. *IEEE Transactions on Robotics*, 30(3):619–630, 2014.

[11] Heather R Martin, Richard W Kimball, Anthony M Viselli, and Andrew J Goupee. Methodology for wind/wave basin testing of floating offshore wind turbines. *Journal of Offshore Mechanics and Arctic Engineering*, 136(2):020905, 2014.

[12] Ryuta Ozawa, Hiroaki Kobayashi, and Kazunori Hashirii. Analysis, classification, and design of tendon-driven mechanisms. *IEEE transactions on robotics*, 30(2):396–410, 2014.

[13] Thomas Sauder, Valentin Chabaud, Maxime Thys, Erin E. Bachynski, and Lars O. Sæther. Real-time Hybrid Model Testing of a Braceless Semi-submersible Wind turbine. Part I: The HyHybrid Approach. In *Proc. of 35th OMAE conf.*, 2016.

[14] Hamid D Taghirad. *Parallel robots: mechanics and control*. CRC press, 2013.

[15] Xiaoqiang Tang. An overview of the development for cable-driven parallel manipulator. *Advances in Mechanical Engineering*, 6:823028, 2014.

[16] Maxime Thys, Lene Eliassen, Valentin Chabaud, Thomas Sauder, Lars O. Sæther, and Øyvind B. Magnussen. Real-time Hybrid Model Testing of a semi-submersible 10MW floating wind turbine, including extreme design cases. In *Proc. of 1st IOWTC conf.*, 2018 (to be published).

[17] Fabian F Wendt, Amy N Robertson, Jason M Jonkman, et al. Fast model calibration and validation of the oc5-deepcwind floating offshore wind system against wave tank test data. In *The 27th International Ocean and Polar Engineering Conference*. International Society of Offshore and Polar Engineers, 2017.